Leakage radiation microscope for observation of non-transparent samples

Juan M. Merlo,[1,*] Fan Ye,[1,2] Michael J. Burns,[1] and Michael J. Naughton[1]

[1] Department of Physics, Boston College, Chestnut Hill, Massachusetts 02467, USA
[2] Present address: LASSP, Department of Physics, Cornell University, Ithaca, New York, 14850, USA
[*]juan.merlo@bc.edu

Abstract: We describe a leakage radiation microscope technique that can be used to extend the leakage radiation microscopy to optically non-transparent samples. In particular, two experiments are presented, first to demonstrate that acquired images with our configuration correspond to the leakage radiation phenomenon and second, to show possible applications by directly imaging a plasmonic structure that previously could only be imaged with a near-field scanning optical microscope. It is shown that the measured surface plasmon wavelength and propagation length agree with theoretically-calculated values. This configuration opens the possibility to study important effects where samples are optically non-transparent, as in plasmonic cavities and single hole plasmonic excitation, without the use of time-consuming near-field scanning optical microscopy.

© 2014 Optical Society of America

OCIS codes: (180.0180) Microscopy; (240.6680) Surface plasmons.

References and links

1. D. Mynbaev and V. Sukharenko, "Plasmonic-based devices for optical communications," Int. J. Hi. Spe. Elec. Syst. **21**(01), 1250006 (2012).
2. Y. Fu, X. Hu, C. Lu, S. Yue, H. Yang, and Q. Gong, "All-optical logic gates based on nanoscale plasmonic slot waveguides," Nano Lett. **12**(11), 5784–5790 (2012).
3. I. Sorger, Z. Ye, R. F. Oulton, Y. Wang, G. Bartal, X. Yin, and X. Zhang, "Experimental demonstration of low-loss optical waveguiding at deep sub-wavelength scales," Nat. Commun. **2**, 331 (2011).
4. H. Raether, *Surface Plasmons on Smooth and Rough Surfaces and on Gratings* (Springer, 1988).
5. S. I. Bozhevolnyi and V. Coello, "Elastic scattering of surface plasmon polaritons: modeling and experiment," Phys. Rev. B **58**(16), 10899–10910 (1998).
6. S. T. Koev, A. Agrawal, H. J. Lezec, and V. A. Aksyuk, "An efficient large-area grating coupler for surface plasmon polaritons," Plasmonics **7**(2), 269–277 (2012).
7. P. Bharadwaj, A. Bouhelier, and L. Novotny, "Electrical excitation of surface plasmons," Phys. Rev. Lett. **106**(22), 226802 (2011).
8. F. Ye, J. M. Merlo, M. J. Burns, and M. J. Naughton, "Optical and electrical mappings of surface plasmon cavity modes," Nanophotonics **3**(1-2), 33–49 (2014).
9. E. S. Kwak, J. Henzie, S. H. Chang, S. K. Gray, G. C. Schatz, and T. W. Odom, "Surface plasmon standing waves in large-area subwavelength hole arrays," Nano Lett. **5**(10), 1963–1967 (2005).
10. J. Lin, J. P. B. Mueller, Q. Wang, G. Yuan, N. Antoniou, X. C. Yuan, and F. Capasso, "Polarization-controlled tunable directional coupling of surface plasmon polaritons," Science **340**(6130), 331–334 (2013).
11. J. W. P. Hsu, "Near-field scanning optical microscopy studies of electronic and photonic materials and devices," Mater. Sci. Eng. **33**(1), 1–50 (2001).
12. R. Esteban, R. Vogelgesang, and K. Kern, "Full simulations of the apertureless scanning near field optical microscopy signal: achievable resolution and contrast," Opt. Express **17**(4), 2518–2529 (2009).
13. H. Wei, D. Ratchford, X. E. Li, H. Xu, and C. K. Shih, "Propagating surface plasmon induced photon emission from quantum dots," Nano Lett. **9**(12), 4168–4171 (2009).
14. E. J. R. Vesseur, R. de Waele, M. Kuttge, and A. Polman, "Direct observation of plasmonic modes in au nanowires using high-resolution cathodoluminescence spectroscopy," Nano Lett. **7**(9), 2843–2846 (2007).
15. S. Massenot, J. Grandidier, A. Bouhelier, G. Colas des Francs, L. Markey, J.-C. Weeber, A. Dereux, J. Renger, M. U. Gonzalez, and R. Quidant, "Polymer-metal waveguides characterization by Fourier plane leakage radiation microscopy," Appl. Phys. Lett. **91**(24), 243102 (2007).
16. I. P. Radko, S. I. Bozhevolnyi, G. Brucoli, L. Martín-Moreno, F. J. García-Vidal, and A. Boltasseva, "Efficient unidirectional ridge excitation of surface plasmons," Opt. Express **17**(9), 7228–7232 (2009).

17. C. Garcia, V. Coello, Z. Han, I. P. Radko, and S. I. Bozhevolnyi, "Experimental characterization of dielectric-loaded plasmonic waveguide-racetrack resonators at near-infrared wavelengths," Appl. Phys. B **107**(2), 401–407 (2012).
18. A. Hohenau, J. R. Krenn, A. Drezet, O. Mollet, S. Huant, C. Genet, B. Stein, and T. W. Ebbesen, "Surface plasmon leakage radiation microscopy at the diffraction limit," Opt. Express **19**(25), 25749–25762 (2011).
19. O. Mollet, S. Huant, and A. Drezet, "Scanning plasmonic microscopy by image reconstruction from the Fourier space," Opt. Express **20**(27), 28923–28928 (2012).
20. J. Ajimo, M. Marchante, A. Krishnan, A. A. Bernussi, and L. Grave de Peralta, "Plasmonic implementation of a quantum eraser for imaging applications," J. Appl. Phys. **108**(6), 063110 (2010).
21. A.-L. Baudrion, F. de Léon-Pérez, O. Mahboub, A. Hohenau, H. Ditlbacher, F. J. García-Vidal, J. Dintinger, T. W. Ebbesen, L. Martin-Moreno, and J. R. Krenn, "Coupling efficiency of light to surface plasmon polariton for single subwavelength holes in a gold film," Opt. Express **16**(5), 3420–3429 (2008).
22. A. B. Evlyukhin, S. I. Bozhevolnyi, A. L. Stepanov, R. Kiyan, C. Reinhardt, S. Passinger, and B. N. Chichkov, "Focusing and directing of surface plasmon polaritons by curved chains of nanoparticles," Opt. Express **15**(25), 16667–16680 (2007).
23. J. J. Burke, G. I. Stegeman, and T. Tamir, "Surface-polariton-like waves guide by thin, lossy metal films," Phys. Rev. B **33**(8), 5186–5201 (1986).
24. F. Ye, M. J. Burns, and M. J. Naughton, "Plasmonic halos-optical surface plasmon drumhead modes," Nano Lett. **13**(2), 519–523 (2013).
25. J. J. Grandidier, G. C. des Francs, S. Massenot, A. Bouhelier, L. Markey, J. C. Weeber, C. Finot, and A. Dereux, "Gain-assisted propagation in a plasmonic waveguide at telecom wavelength," Nano Lett. **9**(8), 2935–2939 (2009).
26. S. A. Maier, *Plasmonics. Fundamentals and Applications* (Springer, 2007).
27. P. B. Johnson and R. W. Christy, "Optical constants of noble metals," Phys. Rev. B **6**(12), 4370–4379 (1972).
28. Q. Wang, J. Bu, and X.-C. Yuan, "High-resolution 2D plasmonic fan-out realized by subwavelength slit arrays," Opt. Express **18**(3), 2662–2667 (2010).
29. S. P. Frisbie, C. F. Chesnutt, M. E. Holtz, A. Krishnan, L. Grave de Peralta, and A. A. Bernussi, "Image formation in wide-field microscopes based on leakage of surface plasmon-coupled fluorescence," IEEE Photonics Journal **1**(2), 153–162 (2009).
30. C. J. Regan, R. Rodriguez, S. C. Gourshetty, L. Grave de Peralta, and A. A. Bernussi, "Imaging nanoscale features with plasmon-coupled leakage radiation far-field superlenses," Opt. Express **20**(19), 20827–20834 (2012).

1. Introduction

In recent years, interactions of light with matter have revealed important physical phenomena with potential utility in a variety of scientific and technical fields, such as optical communication, optical logic and subwavelength manipulation of light [1–3]. One notable such interaction is the surface plasmon (SP), an optically-excited collective oscillation of electrons located at a metal-dielectric interface [4]. Particularly in optics, SPs can be excited in different ways [5–8]. In this context, the near-field scanning optical microscope (NSOM) is the most commonly used tool to study interactions between SPs and matter on subwavelength scales [9, 10]. Even though the spatial resolution of NSOM goes beyond the diffraction limit, this technique has some disadvantages, such as a slow scan rate for image acquisition, limitations in the sample topography [11] and, most importantly, the multiple interactions in the system probe-sample fields that complicate near-field image interpretation [12]. Some alternative non-invasive techniques, such as quantum dot fluorescence (QDF) [13], cathodoluminescence (CL) [14] and leakage radiation microscopy (LRM) [15], have proven reliable tools to be used in place of NSOM. QDF, however, is dependent on the fluorescence time, where the employed particles are active only until becoming bleached [13], while CL requires a specially equipped scanning electron microscope (SEM) to be used, making sample preparation very restrictive [14]. LRM, on the other hand, is a relatively simple technique to implement, with results that are highly reproducible, although the resolution remains diffraction limited [16–18]. Also of great value with LRM is the possibility to obtain direct and Fourier space images at the same time in real-time, when the LRM experimental setup is appropriately adapted [19].

In previously reported work on the LRM technique, the metal sample need to be optically thin. As a result, the illumination source is visible through the sample to the side where the observation is made, which can create false images due to diffraction patterns unrelated to the

plasmonic interactions. Heretofore, the solution to that has been the use of an opaque block positioned at the center of the Fourier plane [19]. In order to overcome the problems associated with the thickness of the metallic sample and the diffraction artifacts, we present here an alternate configuration of an LRM with the capability to study optically non-transparent samples illuminated from the back side, by observing directly onto the sample surface, creating an alternative to the conventional LRM.

In the conventional LRM configuration [18], a sample consists of a thin metallic layer (e.g. ~50 nm thick) deposited onto a glass substrate, decorated with metallic features usually fabricated by electron beam lithography (EBL) [20], focused ion beam (FIB) [21] or direct laser patterning [22]. A tightly focused beam is projected onto the sample to couple SPs on the free metallic surface (as opposed to the substrate-metal surface) [16]. Due to the propagation of the SPs along this surface and the thickness of the metallic layer, there exists radiation that passes through the metallic layer to the glass substrate [18]. This is referred to as leakage radiation, which reaches the substrate at an angle θ_{LR} that is greater than the critical angle (for total internal reflection). Then, in order for the leaked radiation (carrying information of the SP propagation) to be detected in the far field, it is needed to couple from the substrate using immersion oil to a microscope objective with numerical aperture (NA) greater than one [18].

The main differences between our proposed LRM and the conventional configuration are that, for the conventional configuration, observation is made on the glass substrate side of the sample, and the sample is typically optically-thin as commented before. For our configuration, on the other hand, observation is performed directly on the sample surface by use of immersion oil coupling and, more importantly, the metallic coating can be optically thick but SP thin. This last fact is the reason we refer to its use with non-transparent samples.

It is important to note that the dispersion relation in our configuration is the same as for the conventional LRM, with the difference that in our configuration, the SP is excited in a medium S different from air. That is,

$$k_x = k_S \sqrt{\epsilon_S \epsilon_m / (\epsilon_S + \epsilon_m)}, \tag{1}$$

where k_x and k_S are the wavenumbers of the SP at the metallic surface and of the propagating field in S, respectively, while ϵ_S and ϵ_m are the dielectric functions of the dielectric material filling the grating spaces (medium S) and of the metal, respectively [23]. This dispersion relation is valid when the thickness of the metallic layer is much larger than the radiation skin depth. This requirement is fulfilled in the visible frequency range, for example, by a layer of Ag thicker than 100 nm. In such case, there is a solution to the dispersion relation that is radiative in medium S [23], which corresponds to the observed leakage fields in our configuration. In real metals, the dielectric function is a complex number, where the imaginary part represents Ohmic losses. In this sense, from Eq. (1) is clear that k_x is a complex number as well, meaning that the SP is damped in the propagation direction by $\text{Im}(k_x) = k_x''$. Actually, the SP propagation length is defined by $L_{SP} = 1/(2k_x'')$, while $\text{Re}(k_x) = k_x'$ defines the SP wavelength by $\lambda_{SP} = 2\pi / k_x'$.

2. Experimental details

We have adapted an optical microscope (Leica DM6000M) to illuminate the sample from the back side with a laser source of 473 nm wavelength. The sample surface is directly coupled to a 63x microscope objective, with variable NA (0.6 to 1.4), by using immersion oil with calibrated refractive index $n_S = 1.52$. The resulting image is projected onto a CCD camera and acquired by software in true color and real time. The observed field was about $64 \times 48 \ \mu m^2$, but the present work just presents the area of interest in each sample. The proposed

configuration for the acquisition of images in direct space is depicted schematically in Fig. 1(a). In the case of Fourier space images, an additional lens is located in the space between lens L1 and the CCD camera as in the conventional LRM [18].

We have created specialized metal film samples which while optically thick, can allow the coupling of SP from one side of the film to the other. The method used for sample preparation was electron beam lithography (EBL), where a 200 nm thick layer of poly (methyl methacrylate) (PMMA) was spin-coated onto a glass substrate coated with a 70 nm thick layer of ITO. We have called t_{PMMA} and t_{ITO} the thickness of PMMA and ITO, respectively (Fig. 1(b)). After exposure and development, a $t_{Ag} = 150$ nm thick layer of Ag was sputtered onto the sample without any subsequent lift-off process. The result is a metal-coated cavity with the desired geometry and thin metallic vertical walls (70 nm). In our sample, we took advantage of a step-gap leakage coupling method to couple SPs, a method recently reported by our group [24], where resonant plasmonic modes are excited in cavities by the leaked field in thin metallic walls and coupled to the metallic film located at the bottom of such cavities. The main advantage of this kind of sample is that the background illumination (source) is blocked by the optically thick metal, allowing a high signal/background intensity ratio, making the sample clearly distinguishable in direct space. In order to confirm that the presented results were not dependent on the sample structure, a second kind of sample with same parameters the (w, p, t_{ag}) was prepared by focused ion beam (FIB). Results from this experiment are shown in the Appendix.

3. Results

In order to demonstrate the operation and application of our proposed configuration, we have conducted two experiments. First, we used a grating consisting of four ridges of 5 μm length, width $w = 150$ nm, and pitch $p = 440$ nm, illuminated with a laser source of wavelength 473 nm. The electric field polarization was chosen to be E_x, perpendicular to the ridges of the grating, to ensure the strongest coupling.
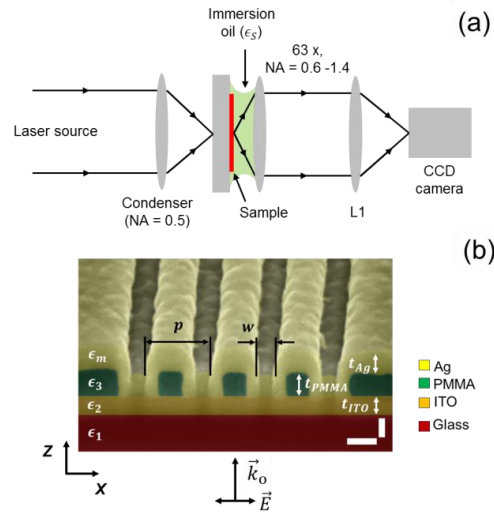

Fig. 1. (a) Schematic LRM experimental setup used for the acquisition of images. (b) SEM image (false color) of the sample structure, where w is the width of the grating and p the pitch; t_{Ag}, t_{PMMA} and t_{ITO} are the thicknesses of the Ag, PMMA and ITO films, respectively. The arrows represent the wave vector $\vec{k}_o$ and electric field of the excitation field $\vec{E}$. The scale bars represent 200 nm in the vertical and horizontal directions and the color chart shows the materials used in the sample.

Figure 2(a) shows the resulting image in true color using NA = 1.4. It is clear that there is evidence for radiating fields on both sides of the grating. These are related to SP propagation along the planar Ag-oil surface away from the grating. On the other hand, in the case of NA = 0.6 (Fig. 2(b)), the grating appeared as a bright rectangle without any of the fine detail of Fig. 2(a). This means that the image of Fig. 2(b) is composed mainly of propagating optical modes of the field produced by SP's resonating in the grating and scattered in the edges of the ridges, as expected due to the low NA. In other words, the bright fringes seen inside the grid areas in both images are due to scattering of optical modes, while the branches left and right of the grating in Fig. 2(a) are due to SP propagation, and not to low-order diffraction produced by such a grating.

In Fig. 2(a), it is clear that the registered intensity is modulated in the x (horizontal) direction. We believe that such modulation is produced by the coherent superposition of far field components produced by the scattering of the SP's created in the grating. In order to experimentally measure the period of the modulation shown in Fig. 2(a), we made a transversal cut in the dashed line and the result is shown in Fig. 2(c). By using the profile shown in Fig. 2(c), it is possible to measure the spatial frequency of the modulation by calculating the power spectrum of the profile. Figure 2(d) shows the result normalized to k_o (excitation wavelength). Thus, the modulation has NA = 0.75 ± 0.01 that is related with common far field interference as stated before. Due to the attenuated propagation of the SP's, it is possible to calculate $k_x^{''}$ by measuring the exponential decay constant of the profile shown in Fig. 2(c). If such a profile is fitted (red line), the measured exponential decay constant is exactly L_{SP}, that in our case corresponds to $k_x^{''} = (0.03 \pm 0.01) k_o$. Latter in the manuscript, we show a second measure of $k_x^{''}$ and the theoretical confirmation of such a value.

It is well established that LRM can detect only the E-field component of the SP that is parallel to the metal-dielectric interface, where it is coupled [18], *i.e.* the existence of this SP is detected by virtue of it leaking into the far field as optical radiation. In this way, we can experimentally obtain $k_x^{'}$ and $k_x^{''}$ in a second way. For this purpose, we studied the Fourier space and the result is presented in Fig. 3(a), where the white circle represents NA = 1.4 (objective NA), while the red and orange are NA = 1 (k_o) and NA = 0.5 (condenser NA), respectively. In Fig. 3(a), it is clear that the central region is related with the scattering of SP's on the edges of the ridges, because it is confined to the region NA ≤ 0.5, it means the illumination NA, confirming the origin of the image shown in Fig. 2(b). Next, we found two symmetric structures located at NA = 1.31 ± 0.01, that correspond to $k_x^{'} = (1.31 \pm 0.01) k_o$. Finally, two bright lobes appeared at NA = 0.75 ± 0.01 that are related with the far field modulation observed in Fig. 2(a).

In order to measure $k_x^{''}$ in the Fourier space image, we made a transversal cut in the intensity defined by the yellow line in Fig. 3(a) and presented in Fig. 3(b). The value of $k_x^{''}$ was calculated from the relationship $k_x^{''} = A/2$, where A is the width of the intensity profile (supposing a Lorentz shape) at full width at half maximum (FWHM) [25], resulting in $k_x^{''} = (0.03 \pm 0.01) k_o$, confirming the value measured before.

In order to cross check our experimental results, we used the dispersion relation calculated for an asymmetric periodic grating [26], stated as follows:

$$\sqrt{k_x^2 - k_o^2} = \frac{k_0 w}{p} \tan(k_o h),\qquad(2)$$

with w and p the parameters of the grating discussed above and h the height of the groves, *i.e.* $h = 100$ nm. Even when Eq. (2) is generally valid for the case $k_o w \ll 1$, it remains a good approximation for the present case. Using exact experimental values of w, p, h, we found that $k_x^{'} = 1.31 k_o$. On the other hand, for the theoretical calculation of $k_x^{''}$, we used again Eq. (1) with ϵ_S (immersion oil) and ϵ_m (Ag) from [27], resulting $k_x^{''} = 0.03 k_o$. It is important to note that all the theoretical values agree closely with the experimental values.
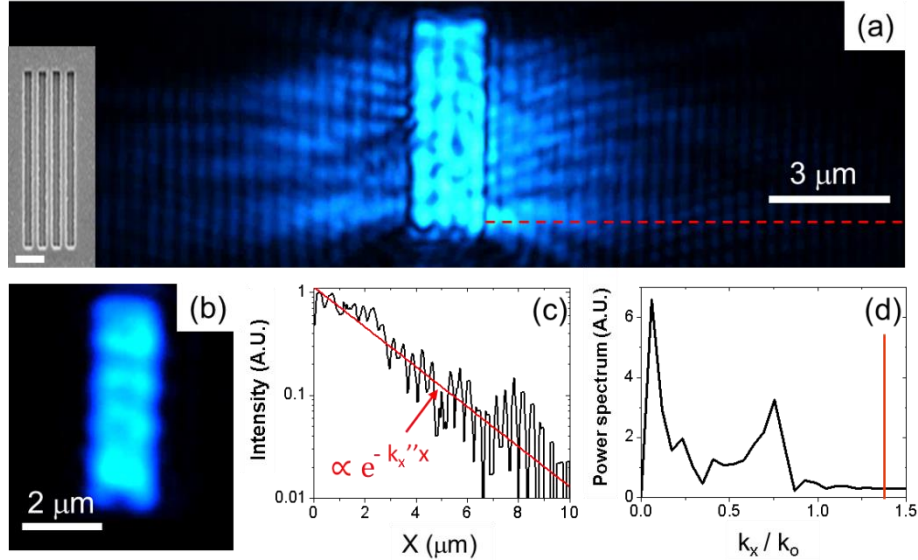

Fig. 2. LRM image acquired by the proposed configuration using NA = 1.4 (a) and far field image using NA = 0.6 (b). The excitation wavelength was 473 nm. The inset to (a) is an SEM image of the grating with w = 150 nm and p = 440 nm. Inset scale bar: 1 μm. (c) Intensity registered in the red line in (a) using logarithmic scale. The red arrow shows an exponential decay shape. (d) Power spectrum calculated from the intensity profile shown in (c). The red line shows the maximum used NA.

For the second experiment, we fabricated a plasmonic cavity by using four gratings with the same length, width w, pitch p and thickness of the layers (t_{Ag}, t_{PMMA}, t_{ITO}) above, disposed on the sides of a square rotated 45° with respect to the horizontal. An SEM image of this structure can be seen in the inset to Fig. 4(a). Here, we used the aforementioned experimental setup. As in the case of a single grating, each grating couples SP's in the perpendicular direction to its ridges on both sides of the grating, Fig. 2(a). The counter-propagating SP's in the inner part of the cavity interfere, generating a two-dimensional standing wave that can be visualized as a square grid-like pattern, shown in Fig. 4(a). A magnified view of the dashed rectangle of Fig. 4(a) is presented in Fig. 4(b).

The intense lobes in the pattern have average widths of $(2.62 \pm 0.01) k_o$, measured as FWHM (red arrows in Fig. 4(c)) and separated by an average distance of $(1.49 \pm 0.01) k_o$. This configuration reproduces results recently reported, where a plasmonic cavity, similar to our sample, is illuminated from the back side and studied by NSOM [28]. The pattern obtained there has the same properties as our results, just scaled by the wavelength and grating size.
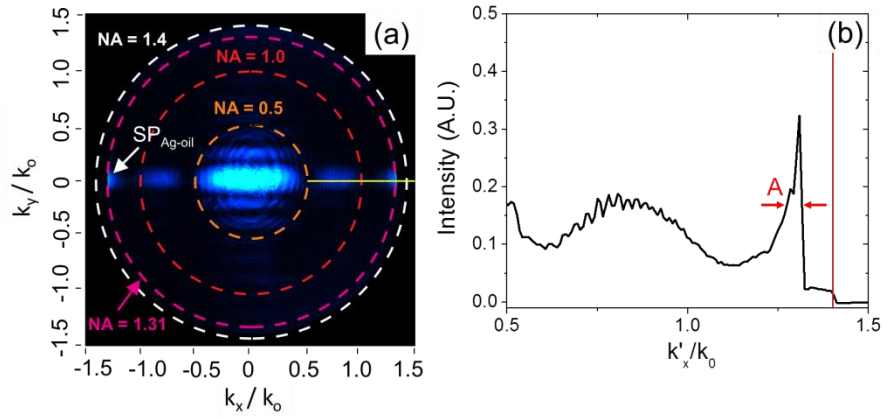
Fig. 3. (a) Fourier space image normalized to the excitation wavenumber of the leaked field in Fig. 2(a). The white circle represents NA = 1.4, while red and orange circles are NA = 1 and 0.5, respectively. (b) Transversal cut made in the yellow line in (a). The arrows represent the distance A measured at FWHM.

As before, we studied the Fourier space of the produced field showed in Fig. 4(a) and the result is shown in Fig. 5(a). The slight asymmetry of the image is due to misalignments of the laser source and the sample. As in the case of a single grating, the region inside NA ≤ 0.5 contains the propagating components of the field. In this case, the generated patterns are related to interference of the different components of the field, meaning the propagating modes of each grating are superimposed on the field produced by the other gratings. Next, as expected, at NA = 1.31 ± 0.01 there appear four features that are related to k'_x, in a direction perpendicular to the grating ridges; these are SP's non-confined in the cavity (purple circle).

In Fig. 3(a), there was one intense lobe on each side of the image at NA = 0.75 ± 0.01, but in Fig. 5(a) appear three intense lobes, due to coherent interference of the different components of the SP's in each grating. On the other hand, the interference pattern in Fig. 4(a) has discrete frequencies that can be visualized as the intersection points of the displaced wavevector k'_x in each direction (green circles). Actually, the distance between a pair of opposite points is $k_{patt} = (1.49 \pm 0.01) k_o$, *i.e.* the wavenumber of the observed pattern.

Figure 5(b) shows the k-space analysis of the wavevectors that appear in the Fourier space in Fig. 5(a). The presented vectors have the same meaning as in Fig. 3(b) and $\vec{k}_{patt}$ is the wavevector of the interference pattern observed in Fig. 4(a). As the analysis has indicated, it is possible to define $\vec{k}_{patt} = \vec{G} + \vec{k}'_x$. In this way, due to each grating-launched SP's, the resulting pattern wavevectors are combined (subtracted) to yield zero (green arrows in Fig. 5(b)), *i.e.* an standing wave, but the distance from point A to A' is the wavenumber of the observed pattern. Finally, it is important to note that in the presented k-space, we have shown just two gratings and their analyses in order to allow an easier visualization of the described situation, but the real case has four directions, as shown in Fig. 5(a).
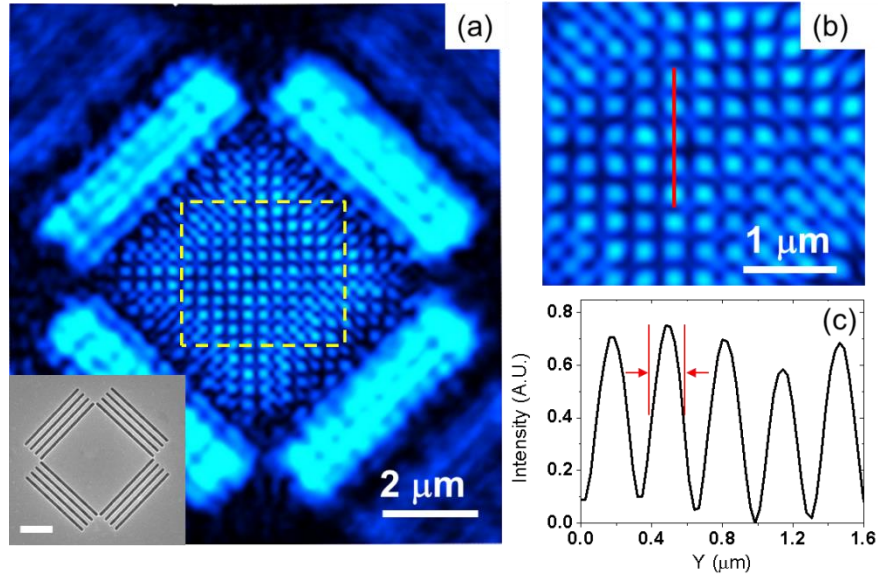
Fig. 4. (a) Optical image taken with the proposed LRM of a plasmonic cavity composed of four perpendicular gratings with width 150 nm and pitch 440 nm. The excitation wavelength was 473 nm. The inset is an SEM image, with a 2 μm the scale bar. (b) Detailed view inside the dashed rectangle in (a). (c) Intensity profile measured along the red line in (b), showing the FWHM.

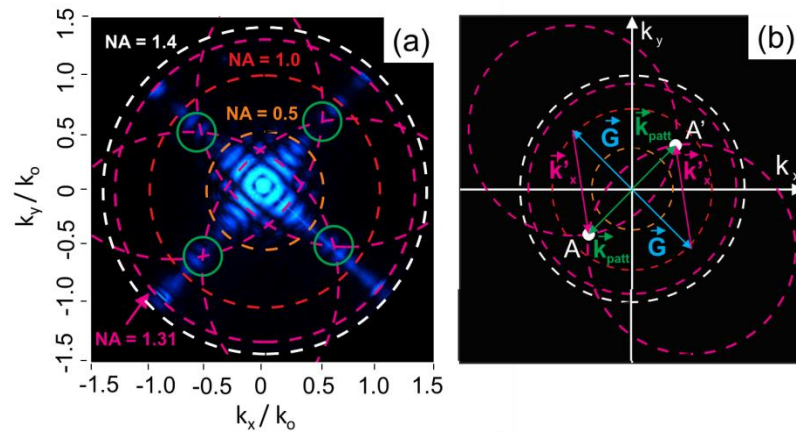Fig. 5. (a) Fourier space image of the plasmonic cavity presented in Fig. 4(a). The orange, red, purple and white circles are associated with NA = 0.5, 1.0, 1.31 and = 1.4, respectively, as indicated. The purple dashed lines are related to $k_x^{'}$ displaced by $\vec{G}$. (b) k-space analysis of experimental Fourier space image in (a). The scale has been changed in order to allow the observation of the complete scheme, but the proportion is the same. The vectors $\vec{G}$, $\vec{k}_x^{'}$ and $\vec{k}_{patt}$ are the wavevectors of the grating, SP and the observed pattern respectively. The distance between points A and A' shows the wavenumber of the observed pattern.

4. Discussion and conclusions

The important characteristic of the leakage radiation microscope technique presented here is that the sample does not allow the transmission of light coming directly from the source, such that the detected light is due to plasmonic coupling in the gratings. Since we are using the step-gap leakage coupling method [24], light detected inside the region with NA ≤ 0.5 is due

to scattering of SP's at the edges of the gratings, due to the sample roughness and probably also due to some impurities in the immersion oil. This LRM technique avoids the necessity of blocking items in the optical path of the detected field (as in dark field microscopy) use in conventional LRM which can potentially produce diffraction artifacts. Actually, the non-necessity of the blocking items has been already reported getting high resolution results [29, 30].

In conclusion, we have shown that a leakage radiation microscope can be configured to directly observe the surface of a non-transparent sample. Our experimental results agree closely with those predicted theoretically. Although observations are made in the frame of a diffraction-limited system, the information extracted from the acquired images shows that such images are related to surface plasmons propagating along the sample surface. It is important to note that the observation field is about 64×48 μm^2, which allows for observation of relatively large area samples, and more important, without the need for scanning as would be required with NSOM. Finally, the proposed configuration opens the possibility to study, among others, the effects of resonant modes as in the case of plasmonic cavities, a phenomenon that requires principally a non-transparent sample.

Appendix

Sample preparation

The sample was prepared by ion milling (FIB) of a 150 nm thickness Ag coating onto glass substrate. The geometrical parameters were similar to those reported in the main text, *i.e.* $w =$ 150 nm, $p = 440$ nm, inset in Fig. 6(a). In such image, the contrast is higher because the different scattering rates on the materials, resulting in dark zones for the glass substrate and bright for Ag coated surface.

Results

In order to compare with the results presented above, we repeated the leakage radiation experiment, resulting the image shown in Fig. 6(a). It is clear the lateral branches are related with the SP propagation, as reported in the main text. Additionally, Fourier space was observed and the result is shown in Fig. 6(b). The higher intensity is due to the direct transmission of light through the grating. It is clear that the behavior is similar to that reported before, actually, $k_x^{'} = (1.27 \pm 0.01)\, k_o$ and $k_x^{"} = (0.03 \pm 0.01)\, k_o$. The difference was due to the fabrication process, which cannot reproduce identical conditions. The former values coincide with those reported in the main text, concluding that the observed phenomenon is not produced by a specific sample, meaning the step-gap leakage method can be applied as a general method for SP generation.
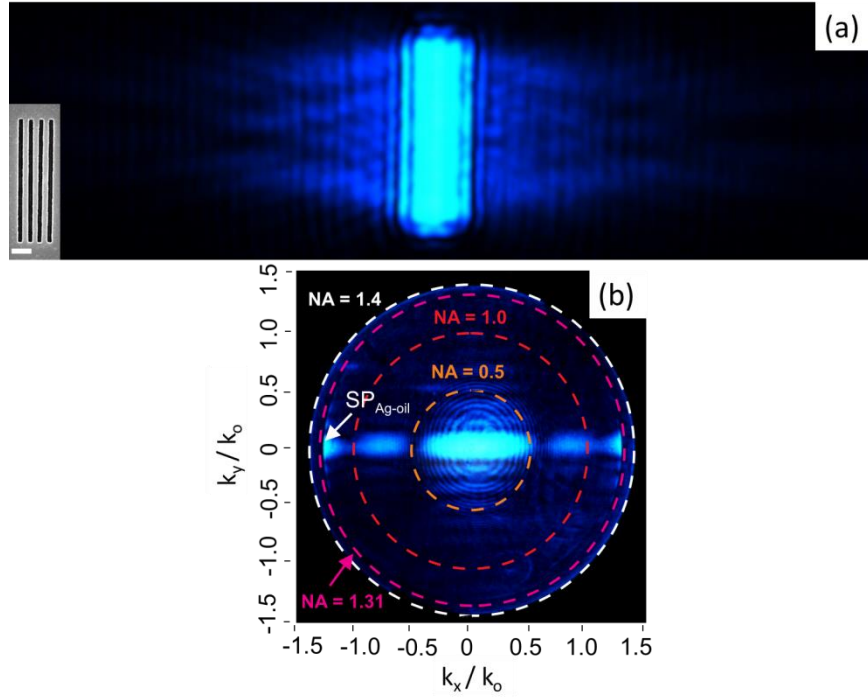
Fig. 6. (a) LRM image acquired by the proposed configuration using a sample made by FIB. The excitation wavelength was 473 nm. The inset to (a) is an SEM image of the grating with w = 150 nm and p = 440 nm; scale bar: 1 μm. (b) Fourier space image of (a) where the circles represent NA = 0.5, NA = 1.0, NA = 1.3 and NA = 1.4, orange, red, purple and white, respectively.